Measurement Report: New particle formation characteristics at an urban and a mountain station in Northern China by Ying Zhou et al.

In this file, the referee comments are in black, our item-by-item replies are in blue, and the corresponding modifications in the manuscript are in red.

Answers to reviewer # 1

NPF is a hot atmospheric topic and its air quality, climate and human health effect still remains not clear. As a measurement report, only 25 days are available, which cannot provide robust statistical results of NPF parameters (frequency, GR and FR). The author compared the NPF parameters with the previous studies in NCP region, however, the short period study can't explain the difference, but cause large uncertainties in statistical values. In this work, something new about the NPF events study should be pointed out as many similar studies have been conducted in the same region in China.

As per suggestion of the referee, we extended our data set at urban Beijing (UB) to include two full summers (from June 1 to August 31) in both 2018 and 2019. With the extended data, we updated our discussion on favorable and limiting factors for NPF event occurrence at the urban Beijing station. We also estimated the size of the area within which regional NPF events occurred during our observations. This estimation could possibly explain the phenomenon that most ending diameters of NPF events during our observation were limited to below 70 nm. Our results highlight the importance of anthropogenic emissions for NPF occurrence and subsequent growth in summer Beijing. Unfortunately, we were not able to include more data from the background mountain station (MT), since no long-term measurements were maintained. Yet, we are able to observe the contribution of the MT in forming particles and its difference from the UB station. Our study highlights the importance of establishing and maintaining long-term measurement not only in urban locations but also in rural ones.

Major concerns:

1. Statistical significance: The statistical numbers of formation rate, growth rate, etc. was calculated based on only a few NPF cases (12, 13 NPF events at different locations). Is this statistical meaningful as the small quantity of cases? Also the comparison of the NPF frequency, GR, FR, and CS with the previous long-term study should be careful.

As mentioned above and as per suggestion of the referee, we extended our data set at urban Beijing station (UB) to include two full summers (from June 1 to August 31) in 2018 and 2019 to improve our statistical conclusions. With the extended data, we found that the shorter observation period between June 14 to July 14, 2019 is representative of the urban Beijing summer as no significant difference in NPF events' properties were observed when comparing the observation from June 14 to July 14, 2019 to the two full summer periods in 2018 and 2019. We then updated the comparison of particle growth rate, formation rate and CS based on the data measured in summer 2018 and 2019 at UB station.

The following discussion and figures (Figure R1-1, Figure R1-2 and Figure R1-3) will be added to the manuscript:

Figure R1-1a shows the difference in CS between NPF event and non-event days during our observation in summer 2018 and 2019 (two whole summers) at UB site and short-term parallel observations at both sites. The 'NPF1' and 'non-event1' referred to NPF and non-event days during the two whole summers, respectively, while 'NPF2' and 'non-event2' referred to NPF and non-event days during the short-term parallel observation period from June 14 to July 14, 2019 at both sites, respectively. The longer-term periods are used for confirming the representativeness of the short-term overlapping period for the whole summer. As shown in the figure, the median CS on NPF1 or NPF2 days is equivalent for UB station (CS_{NPF1} = 0.010s^{-1}; CS_{NPF2}= 0.009s^{-1}) and less than a factor of 1.2 different between non-event1 and non-event2 in UB station ($CS_{nonevent1}$ = 0.023s^{-1}; $CS_{nonevent2}$= 0.020s^{-1}), which confirms the representativeness of our short-term measurement period to the overall urban Beijing summer.

Our results in Fig. R1-1a show that on NPF event days, the median CS was ~ 0.01 s^{-1} during the first 2 hours of the NPF events, at both stations. On common NPF event days, the median

CS was 0.009 s^{-1} at UB station and ~0.01s^{-1} at MT station, respectively. In comparison, on non-event days, during roughly the same time period (9:00–11:00 LT), the CS was substantially higher, with median values of 0.02 s^{-1} and 0.014 s^{-1}, at UB and MT stations, respectively. Figure R1-1b presents the median CS during the first 2 hours of NPF events on common NPF event days measured at both stations, and shows the high correlation between the two.

Figure R1-1c shows the NPF event frequency as a function of CS during our observation at UB site in summer 2018 and 2019 and how the NPF event frequency decreased with increasing CS. When CS was smaller than 0.01 s^{-1}, all days were classified as NPF event days, and when CS was larger than 0.035 s^{-1}, no day was classified as NPF event day. This shows the major role of background particles in controlling the occurrence or inhibition of NPF events as shown in several previous studies in China and internationally (Deng et al., 2020a; Cai et al., 2017; Kulmala et al., 2017). While we cannot present a similar figure from the MT station, the same conclusion applies where CS does play a role in inhibiting NPF observation owing to the difference in the CS values observed between NPF and nonevents at MT in Fig. R1-1a. Yet, since the overall preexisting particle concentration at the MT is rather on the low end, the role of CS might not be as vital at the MT station as for the UB station.

The particle formation rates (J_7) at the two stations during the measurements are presented in Fig.R1-2a. J_7 observed during the short-term parallel observation (NPF2) at UB site was in the range of 3.0-10.0 $cm^{-3}\,s^{-1}$ with a median of 5.4 $cm^{-3}\,s^{-1}$, comparable with those observed in summer 2018 and 2019 (NPF1 = 2-14.0 cm^{-3} s^{-1} with a median of 4.9 cm^{-3} s^{-1}) and significantly higher than the values in the MT station (0.75-3.0 $cm^{-3}\,s^{-1}$ with a median of 0.82 $cm^{-3}s^{-1}$) for common NPF events (Fig.R1-2b).

The particle growth rates in size range of 7-15 nm ($GR_{7\text{-}15nm}$) at the UB station (4.8-12.9 nm/h with a median of 7.8 nm/h) during NPF2 was also comparable with the whole summers (NPF1) (4.8-12.9 nm/h with a median of 8.5 nm/h). While the difference in J_7 was 7 times higher in UB than in MT, the observed GR were only slightly higher at UB than at the MT station (5.7-10.5 nm/h with a median of 6.5 nm/h) for common NPF events (Fig. R1-2c&d), implying that precursors needed for particle formation were much more abundant in the

polluted urban environment (Wang et al., 2013), while those needed for growth are rather comparable.

2. Instrument consistency: in the section 2.2, there is DMPS, SMPS, FMPS used in the PNSD measurement, the comparison of PNSD derived by different instrument should be given of the overlap size range. It is very important to make sure the data are comparable, as the PNSD data also determine the formation rate, growth rate and CS. The type and manufacturer of DMA of DMPS, as well as the SMPS should be also provide.

We thank the reviewer for the suggestions.

The following discussion and figures (Figure R2-1) will be added to the manuscript in section 2.2:

The DMPS consists of consists of one Hauke-type DMA (differential mobility analyzer, home-built by university of Helsinki) in different flow rates and one CPC (condensation particle counter, TSI Model 3772). Details of this instrument can be found in Salma et al., (2011) and Kangasluoma et al. (2020).

At MT station, a scanning mobility particle sizer (SMPS, consists of a TSI Differential Mobility Analyzer model 3081) and a fast mobility particle sizer (FMPS, TSI Model 3091) were used to measure particle number size distribution from June 14 to June 28 and from June 29 to July 14, respectively. The particle number size distribution measured by FMPS correlated well with SMPS after being calibrated (Lee et al., 2013).

To ensure high quality of particle number size distribution data at UB site, a particle number size distribution system (PSD) also sampled in parallel with DMPS from June 1 to August 31, 2019 (summer 2019). It measured particle number size distribution in the size range of 1 nm to 10 μm. It included a nano-scanning mobility particle sizer (nano-SMPS, 3–55 nm, mobility diameter), a long SMPS (25–650 nm, mobility diameter) and an aerodynamic particle sizer (APS, 0.55–10 μm, aerodynamic diameter). Details of this instrument can be seen at Liu et al. (2016) and Deng et al. (2020b).

As shown in Fig. R2-1, median particle number size distribution obtained from PSD and DMPS matched well with each other within a factor of 2 during our observation in summer

2018 and 2019 at UB site. We cannot compare particle number size distribution data obtained from DMPS, SMPS and FMPS as we did not sample with these three instruments in parallel at the same site. However, it is reasonable to assume that particle number size distribution obtained from FMPS were comparable with those from DMPS as on one hand the measurement techniques of particle number size distribution in the size range of these two instruments have been well developed and are applied in quite a lot observations in several environments (Wang et al., 2017;Kangasluoma et al., 2020). On the other hand, the FMPS was carefully calibrated and properly operated during the observation as discussed above. Similar conclusions apply for the SMPS as well, where we can rely on using the measurement from this instrument to discuss at least NPF event frequency at MT site during June 14 to June 28, 2019, during which parameters of only one NPF event are calculated.

3. The influence of air mass origin on the regional NPF occurrence was discussed. As the MT site locates nearby the mountain, how does the topography affect the air mass, local wind, as well as the inhomogeneity of regional NPF events should be also addressed.

We thank the referee for the suggestions. As per suggestions of the referee, the following discussions and figures (Figure R3-1 and Figure R3-2) are added to the manuscript results section:

3.5 Effect of topography

In Figure R3-1 we show average particle number size distribution and particle number concentration on NPF event and non-event days during our short-term parallel observation at both sites. On NPF event days, nucleation and Aitken mode particle number concentrations were much smaller at MT station than those at UB station due to smaller particle formation rates and less anthropogenic emissions. Interestingly, accumulation mode particle number concentrations were higher at MT station (701-2900 cm^{-3}, with a median of 1500 cm^{-3}) than that at UB station (350-1416 cm^{-3} with a median of 700 cm^{-3}) (Fig.R3-1b). Due to the close proximity of the two measurement sites, the air mass arrival directions and source regions were (mostly) similar at both sites throughout the short-term parallel measurement period (Table 1) hence the regional and transported cannot explain the higher accumulation mode

particle number concentration at MT site. As there were few primary emissions at MT site, the accumulation mode particles could be attributed to secondary particles (Kulmala et al., 2021), indicating particles at MT station were more aged than those at UB station (Fig.R3-1a). The possible reason is that mountains block pollution diffusion, which in the end resulted in comparable CS at MT station as UB station.

Figure R3-2 shows an example of the wind distribution before and during NPF event on June 30, 2019 at 850 hPa (close to the altitude of MT station) and 10 m above ground level. As shown in Fig. R3-2, the reanalyzed wind directions at 850 hPa were similar as those at 10 m above the ground level at MT station. Actually, the wind conditions on other NPF event days at MT station during our observation had similar characteristics that the wind directions were similar between 850 hPa and 10 m above ground level indicating air masses well mixed during NPF events. Earlier observations also found NPF event happened uniformly within the mixing layer at their observation stations and particle number size distribution remains roughly constant within the mixing layer (Shen et al., 2018;Lampilahti et al., 2021).

Minor comments:

1. L18-19, I don't think this conclusion is appropriate in the abstract, as the sentence imply this is the first work about urban and regional measurement. Actually, Wang et al., (2013) has reported the regional NPF events in urban Beijing and a regional background site based on one-year dataset before.

We thank the referee for the comments. We agree that our work about urban and regional measurement is not the first but the observations on NPF events on the mountain is still rare in China emphasizing the need of establishing and maintaining such long term observations there.

As per suggestions of the referee, we corrected the sentence in line 18-19 as below:

Most observations on NPF events in Beijing and its vicinity were conducted in populated areas, whereas observations on NPF events in mountain sites with few anthropogenic emissions are still rare in Beijing (Wang et al., 2013). The spatial variation of NPF event intensity has not been investigated in detail by incorporating both urban area and mountain measurements.

2. L47, the reference of the same author should be cited as Guo et al., 2014; 2020.

We corrected the citation as Guo et al., 2014; 2020 in our manuscript.

3. L217, what is "good data"? The clear explanation should be given.

The "good data" meant that particle number size distribution were valid that visual inspection of the data and the number concentrations as well as instrument status do not indicate problems in the measurements at both sites. As per suggestions to the reviewer, we corrected sentence in line 217 as below:

Only days when particle number size distribution data were valid that visual inspection of the data and the number concentrations as well as instrument status do not indicate problems in the measurements for both stations were taken into consideration in our analysis.

4. L222, higher NPF frequency in this study, as compared with Wang et al., 2013; Deng et al., 2020a, was explained by "25 days were validated data", it is not convincing. The short period study caused large uncertainty in the comparison, including the formation rate, growth rate, frequency and CS. However, it can't explain for the higher or lower value. Other favorable parameters for NPF, e.g. meteorology, precursors, CS, should also be taken into consideration.

We thank the referee for the comments. As per suggestions to the reviewer, the following discussions and figures (Fig.R4-1, Fig.R4-2 and Fig.R4-3) will be added in our manuscript:

In Fig.R4-1, we show frequencies of air masses arriving at UB station from different directions during our observation in summer 2018 and 2019. The most frequent air masses arriving at UB station belonged to the South group. During our observation in the two summers, out of 155 days were 52 days belonging to the South group and 39, 32, 9 and 23 days in air masses belong to North, East, West and Local groups, respectively. NPF event frequency with respect to air masses is also shown in Fig. R4-1. It is noticeable that air mass origin influenced the occurrence of NPF events at UB site as the majority of NPF events occurred when the air masses were coming from the north. During our observation in summer 2018 and 2019, 34 (out of 55) NPF events occurred in air masses from the North group and 9, 2, 2 and 6 NPF events in the South, East, West and Local groups, respectively (Fig.R4-1a). One prominent feature of these air masses is their difference in CS. As shown in Fig. R4-1b,

the CS of the air masses classified as the North group (with median values of 0.01 s^{-1} at UB station) is substantially lower than that in other air mass classes (CS = 0.03, 0.025, 0.017, 0.03 s^{-1}, for south, east, west and local, respectively), which might explain the high NPF event frequency associated with this air mass class. During the observation from June 14 to July 14 in summer 2019, the most frequent air masses arriving at both sites belonged to the North group as shown in Table 1. Out of 25 days, there were 8 and 9 days belonging to the North group, at UB and MT sites, respectively. The highest frequency of NPF events also occurred when the air masses were coming from the north. The high NPF events frequency during our observation form June 14 to July 14 could also be attributed to the frequent air masses arriving at both sites from north to Beijing.

In Figure R4-2, we show diurnal variation of meteorological variables during our observation in summer 2018 and 2019 at UB site and observations from June 14 to July 14 in 2019 at UB and MT sites. It is noticeable that the short-term observation compared well with the long-term observation and therefore is representative of summer at UB site as shown in Fig.R4-2.

In Fig. R4-3a, we show the concentration of sulfuric acid as a function of CS during summer 2018 and 2019 at UB site. As shown in Fig. R4-3b, the median sulfuric acid (H_2SO_4) concentrations at UB station were 8.1×10^6 cm^{-3} and 4.5×10^6 cm^{-3} on NPF event days and non-event days, respectively, during observation from June 14 to July 14 in 2019 and 7.9×10^6 cm^{-3} and 3.4×10^6 cm^{-3} on NPF event days and non-event days, respectively, during the observation in summer 2018 and 2019. This suggests that H_2SO_4 was important for NPF events at the UB station (Deng et al., 2020b; Dada et al., 2020b). On the other hand, as shown in Fig.R4-3a, the H_2SO_4 concentration during 9:00- 11:00 (local time) on non-event days could be comparable with that on NPF event days, especially when CS was high. Altogether, our observation shows that the occurrence of NPF events was controlled by both H_2SO_4 and CS at the UB station (Cai et al., 2020).

5. Section 3.1.4, do you mean the higher ending diameter at UB site, supported by the higher condensing vapors? But as you have mentioned, the GR at both sites were comparable, does that mean the condensing level are also comparable? The conclusions from GR and ending

diameter were not consistent, it should be discussed further.

We thank the referee for the comments. We found that the ending diameters were slightly higher at UB site than at MT site, but the difference is not significant (49 nm vs 45 nm), in addition, the GR on common NPF event days were a little bit higher at UB site than MT site. Earlier research pointed out that in order to observe the growth until 100 nm at the measurement station under typical conditions, simultaneous NPF should happen in a very large area (e.g. with wind speed 5m/s and growth rate of 3nm/h from the station to roughly 600 km upwind from the station) (Paasonen et al., 2018). To discuss the ending diameters, we evaluated the size of regions that NPF events could be occurring during our observation. Also, as per suggestions of the reviewer, we updated our comparison of GR on common NPF events as well as the discussion on ending diameters as follows:

The particle growth rates in size range of 7-15 nm ($GR_{7\text{-}15nm}$) at the UB station (4.8-12.9 nm/h with a median of 7.8 nm/h) during observation from June 14 to July 14, 2019 was also comparable with that during the observation in summer 2018 and 2019, a little bit higher than that in the MT station (5.7-10.5 nm/h with a median of 6.5 nm/h) for common NPF events (Fig.R1-2c&d), implying that precursors were only slightly more abundant in the polluted urban environment (Wang et al., 2013).

Addition to the methods' section:

2.4 Estimating the spatial extent of NPF

The observation of regional new particle formation events, where the growth of newly formed particles can be followed for several hours, is a result of NPF taking place over a large spatial area. This is because as time progresses, the particles observed at a measurement site must have originated from further and further away due to non-zero wind conditions. Following the progression of the observed NPF event and using air mass back trajectories, we can estimate where the particles observed at different stages of the NPF event were initially formed by calculating the air mass locations at the onset time of the NPF event (assuming that NPF occurs simultaneously over the larger area). Typically, the mode related to the NPF event disappears from the observations after some time. This is an indication of the currently observed air mass arriving from an area where NPF was no longer taking place due to

unfavorable local conditions. If the shift in the air mass origin towards unfavorable conditions occurs gradually over time, the mode related to the NPF event can enter a stage of growth stagnation (or even decrease in size) before disappearing completely (Kivekäs et al., 2016). This is because the increasing transport time between NPF onset and observation of the particles at the measurement site provides less and less additional 'material' for aerosol growth towards the more unfavorable conditions. Calculating the locations where NPF is assumed to have taken place for longer data sets including several regional NPF events can give an estimation of the typical spatial extent of NPF around the measurement location. It should be noted that even in relatively clear cases, the subjective determination of NPF event onset and end times can easily lead to uncertainties of few tens of kilometers in the estimations. In locations with strong primary pollution sources, such as urban Beijing, objective determination of said times becomes even more difficult. More details and discussion related to the method and its uncertainties can be found in Kristensson et al. (2014).

Results of the NPF spatial analysis are shown in Figure R5-3 and discussed in section 3.4 below.

Addition to Results section:

3.4 Ending diameters of newly-formed grown particles

Earlier observations have shown that diameters of newly-formed particles should be larger than 70 nm to contribute to cloud condensation nuclei significantly (Man et al., 2015;Ma et al., 2021) and will be considered as haze particles when their size reaches larger than 100 nm (Kulmala et al., 2021). In Fig. R5-2, we show ending diameters (End Dp) of newly formed grown particles during our observations at both sites. End Dp during the observation from June 14 to July 14 at UB site (21-105 nm, with a median of 49 nm, Fig.R5-2a) had similar characteristics as those during the long-term observation in summer (21-126 nm, with a median of 56 nm, Fig.R5-2a) where most of the End Dp were in the range of 25-70 nm. As shown in Fig.R5-2b, 61% of End Dp were in the range of 25-70 nm, and only 9% of End Dp were larger than 100 nm during our observation in summer 2018 and 2019 at UB site. We

found that the ending diameters were slightly higher at UB site than MT site, but the difference is not significant (49 nm vs 45 nm) as shown in Fig. R5-2c.

Earlier research has pointed out that in order to observe particle growth until 100 nm at a measurement station under typical conditions, simultaneous NPF should happen over a very large area (e.g. with wind speed 5 m/s and growth rate of 3 nm/h from the station to roughly 600 km upwind from the station) (Paasonen et al., 2018). During our observation in summer 2018 and 2019, most of the newly formed modes kept growing for about 20 hours after an NPF event started, and the maximum horizontal extension of the observed NPF events in the growth stage is restricted to within about 200 km (~2° in latitude) north of UB site (Fig. R5-3). As shown in Fig. R5-3, the population density is also higher within the area extending ~200 km north than beyond this limit. Therefore, it seems that NPF events were limited to the regions with some contribution from anthropogenic emissions during air mass transport from north to Beijing. Roughly similar extent of the NPF area is also seen in other directions. However, towards the south it is more likely that increasing condensation sink from accumulating pollution becomes the limiting factor for NPF occurrence rather than decreasing strength in emission sources. NPF events at MT station had similar characteristics as those at UB station with the NPF event region extending a few hundred kilometers towards the north. The NPF events in this direction were disrupted after a relatively similar distance (or they enter the growth stagnation phase, which will be discussed in section 3.6.3). The limited NPF event area could possibly explain why most End Dp we observed were smaller than 70 nm.

3.6.3 Growth stagnation and decreasing mode diameter case during our observations

During our observations in summer 2018 and 2019 at urban site and the observation from June 14 to July 14, 2019 at MT site, there were some cases where the newly-formed particles entered a phase of growth stagnation or even displayed a decreasing mode diameter. On June 30, 2019 such case occurred simultaneously at both sites and we chose this day for a case study.

As shown in Fig.R5-4 a&b, the newly-formed particles entered a phase of growth stagnation almost at the same time around 12:00 at both sites. Particle mode diameters decreased from

31 nm to 15 nm at UB station around 15:00, under relatively calm meteorological condition, indicating that meteorological condition could not be the reason for particle sizes decrease on June 30, 2019 at both sites. Around the same time, mode diameter at MT station also decreased gradually from 25 nm to 16 nm. Earlier observations in summer-time Beijing have speculated mode diameter decrease to be related to particle evaporation, which is triggered by favorable meteorological conditions e.g. increasing wind speed or temporal changes and vapor dilution (Zhang et al., 2016). From Fig. R5-3 we see, that the air masses observed during the growth stagnation or diameter decrease (both marked under growth stagnation in the figure) were often located quite far in the north over the less populated areas during the onset time of regional NPF. It is also possible, that the less favorable initial conditions for particle formation and growth over these areas, combined with increasing wind speed or temporal changes in the growth rate, could explain the observations of decreasing particle sizes without evaporation (Kivekäs et al., 2016; Hakala et al., 2019).

6. Figure 1: why the station of S60 is shown in the figure?

We thank the referee for the comments. The S60 referred to the location where particles formed during the non-local NPF event observed at MT station on June 15, 2019.

We added the following sentence in our manuscript:

Figure 1: Map showing locations of urban station (UB), Longquan station (LQ), mountain station (MT) and another site 60 km south from MT station (S60). The S60 referred to the location where particles formed during the non-local NPF event observed at MT station on June 15, 2019. Image is produced using © Google Maps.

7. The key word: haze, there is no much discussion about how NPF event contributing to regional haze formation in the study. So I think this key word is not appropriate.

We thank the referee for the comments. As per suggestion to the reviewer, we removed the key word “haze”.

Figures

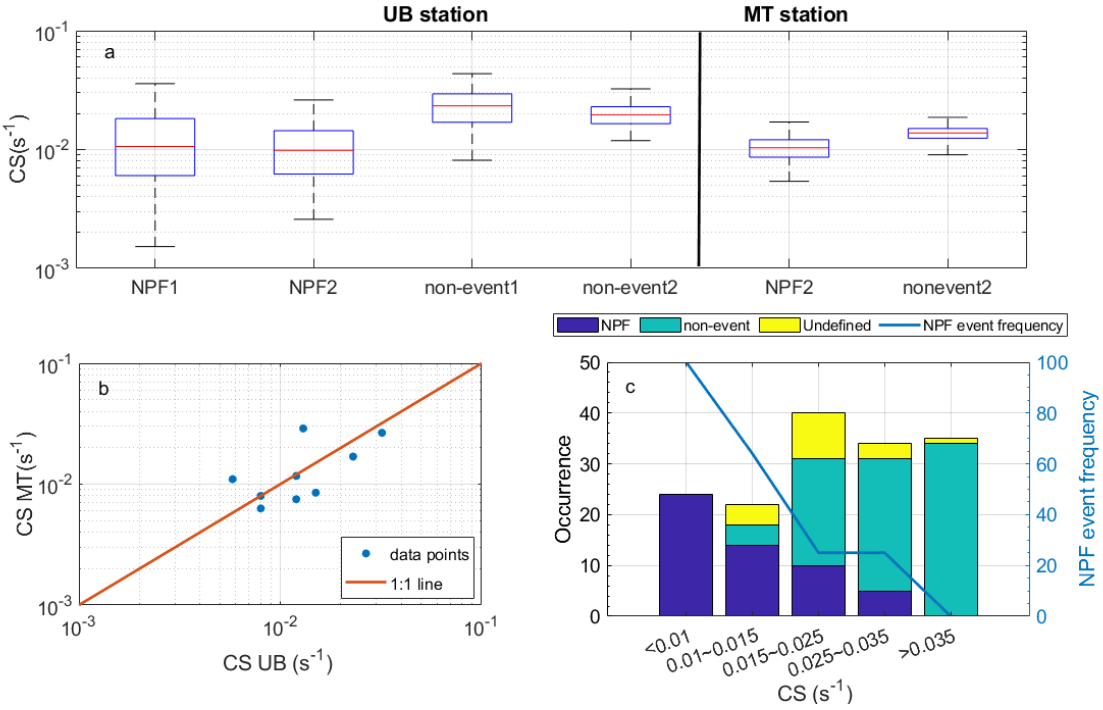

Figure R1-1: (a) Median and percentiles of condensation sink (CS, s^{-1}) during our observations at both stations. The 'NPF1' and 'non-event1' referred to NPF and non-event days during summer 2018 and 2019, while 'NPF2' and 'non-event2' referred to NPF and non-event days during the short-term parallel observation from June 14 to July 14, 2019 at both sites. The red line represents the median of the data and the lower and upper edges of the box represent 25th and 75th percentiles of the data, respectively. The length of the whiskers represents 1.5× interquartile range which includes 99.3% of the data. The time resolution of CS was 8 min. (b) Median CS during the first 2 hours of NPF events on common NPF event days measured at both stations (MT vs. UB). (c) Numbers of NPF event, non-event and undefined days as well as NPF event frequency as a function of CS during our observation in summer 2018 and 2019 at UB station.

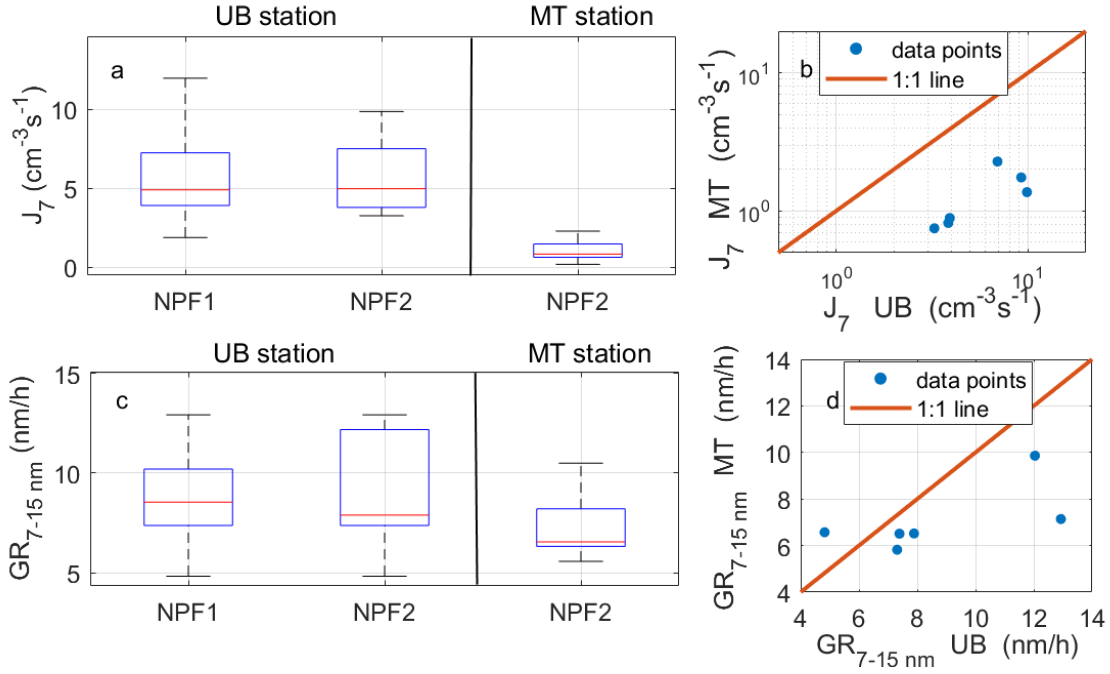

Figure R1-2: Median and percentages of particle formation rates of 7 nm (J_7, $cm^{-3}s^{-1}$) (a) and particle growth rates from 7 to 15 nm ($GR_{6\text{-}15\ nm}$, nm/h) (c) measured at both stations during our observation as well as comparison between J_7 (b) and $GR_{6\text{-}15\ nm}$ (d) of common NPF events. The red line represents the median of the data and the lower and upper edges of the box represent 25th and 75th percentiles of the data, respectively. The length of the whiskers represents 1.5× interquartile range which includes 99.3% of the data. The 'NPF1' and 'non-event1' referred to NPF event and non-event days in summer 2018 and 2019 and the 'NPF2' and 'non-event2' referred to NPF event and non-event days during the observation from June 14 to July 14, 2019.

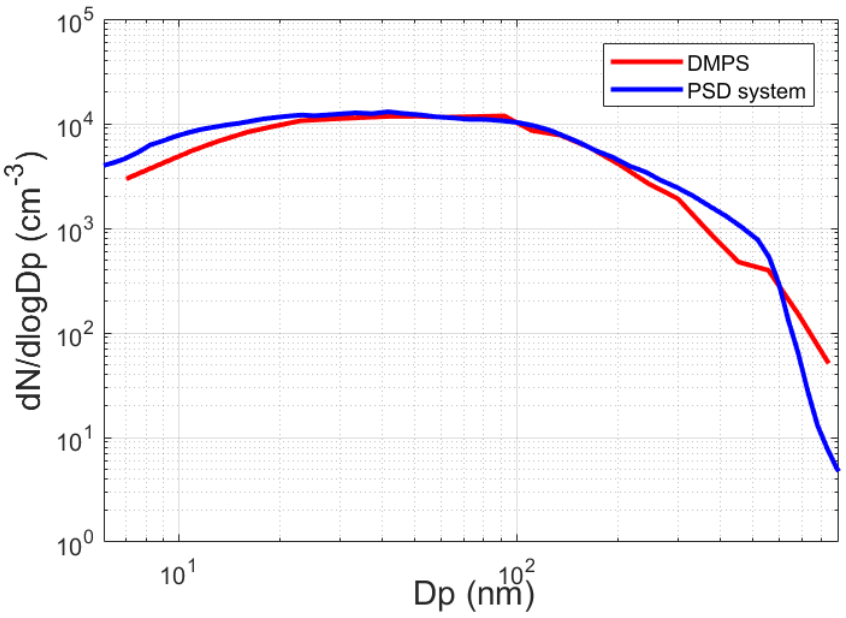

Figure R2-1: Median particle number size distribution in 5-900 nm measured by DMPS and PSD during our observation from June 1 to August 31, 2019 at UB station. The time window of the data is from 9:00-15:00 of every day.

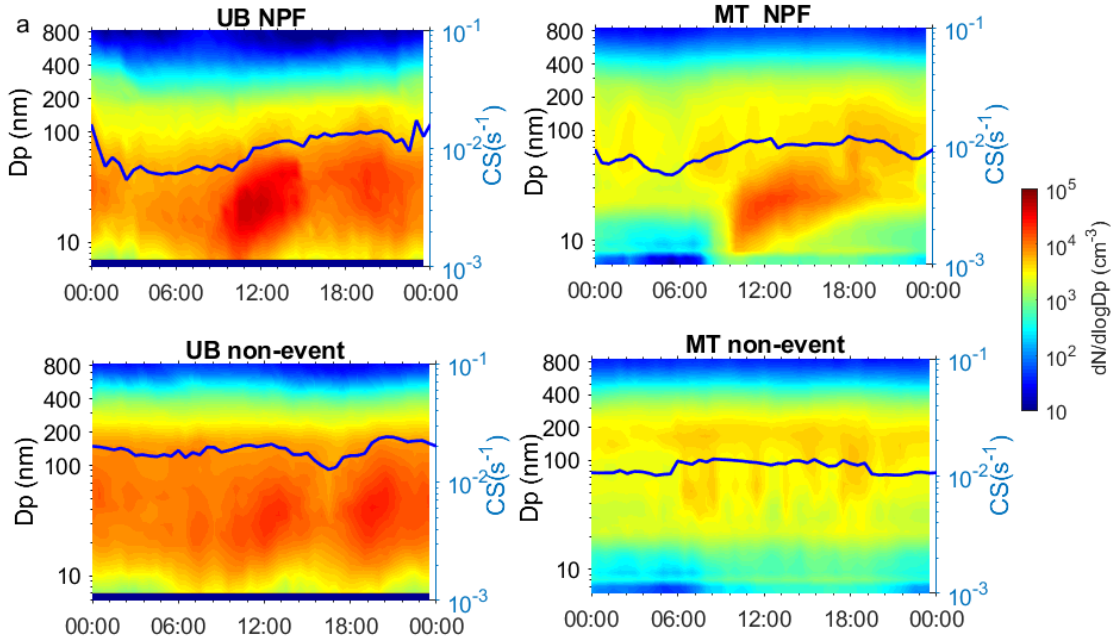

Figure R3-1: (a) Median particle number size distribution as well as CS (blue lines) on NPF event and non-event days at UB (left panel) and MT (right panel) stations and (b) median and percentiles of nucleation, Aitken and accumulation modes particle number concentration on NPF event and non-event days during our observation from June 14 to July 14, 2019 at both stations. The red line represents the median of the data and the lower and upper edges of the box represent 25th and 75th percentiles of the data, respectively. The length of the whiskers represents 1.5× interquartile range which includes 99.3% of the data. Data outside the whiskers are considered outliers and are marked with red crosses.

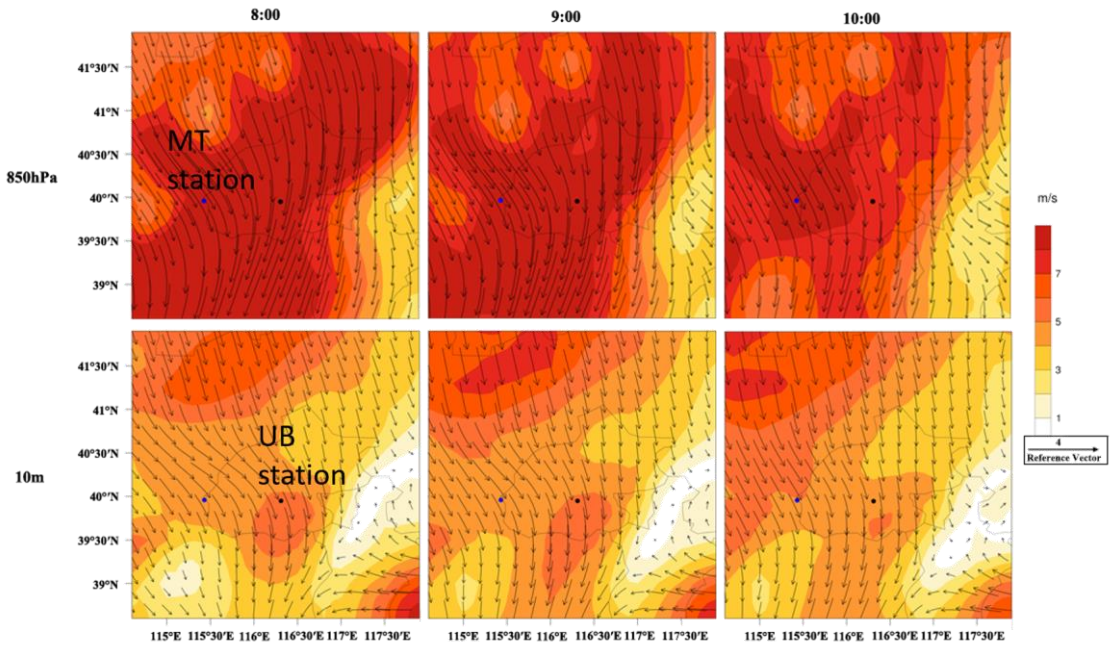

Figure R3-2: Wind distribution at 8:00, 9:00 and 10:00 on June 30, 2019 at 10 m above the ground level and 850 hPa (close to the altitude of MT station). The blue and black points on the figures represent MT and UB stations, respectively.

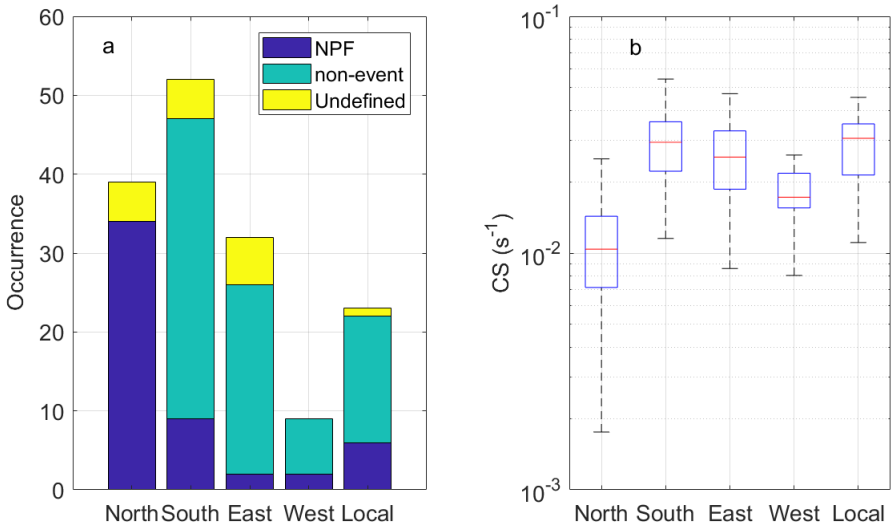

Figure R4-1: Occurrence of NPF events and non-events under air masses arriving from different directions (a) as well as medians and percentiles of condensation sink (CS, s^{-1}) during the 9:00-11:00 (local time) under different air masses (b) during our observation in summer 2018 and 2019 at UB station. The red line represents the median of the data and the lower and upper edges of the box represent 25th and 75th percentiles of the data, respectively. The length of the whiskers represents 1.5× interquartile range which includes 99.3% of the data. Data outside the whiskers are considered outliers and are marked with red crosses. The time resolution of CS was 8 min.

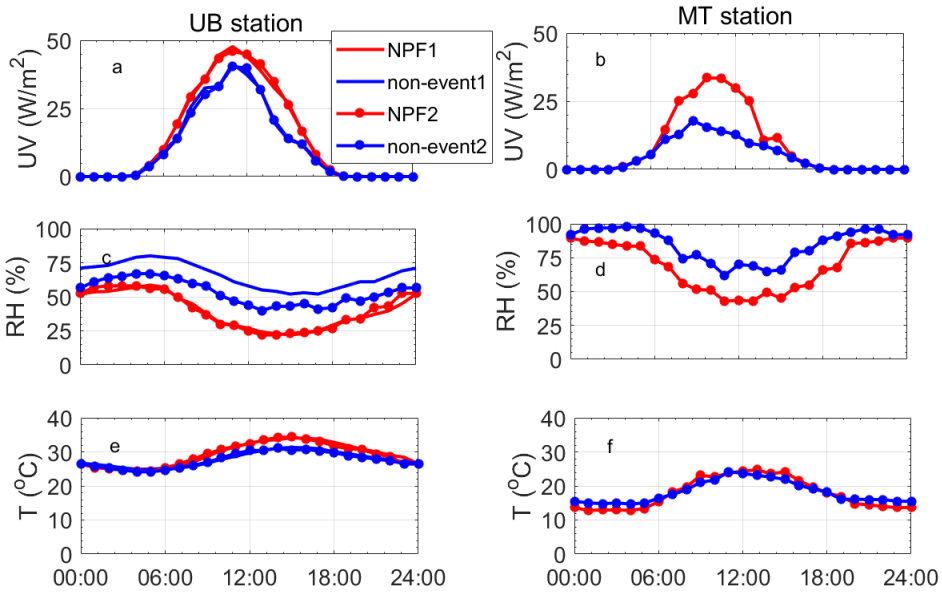

Figure R4-2: (a, b) Diurnal pattern of solar radiation (UV, W/m^2), (c, d) Temperature (T, ℃), and (e, f) Relative humidity (RH, %), at UB (left panel) and MT (right panel) stations on both NPF event and non-event days. Time resolutions for all data points here were 1h. The 'NPF1' and 'non-event1' referred to NPF event and non-event days in summer 2018 and 2019 and the 'NPF2' and 'non-event2' referred to NPF event and non-event days during the observation from June 14 to July 14, 2019.

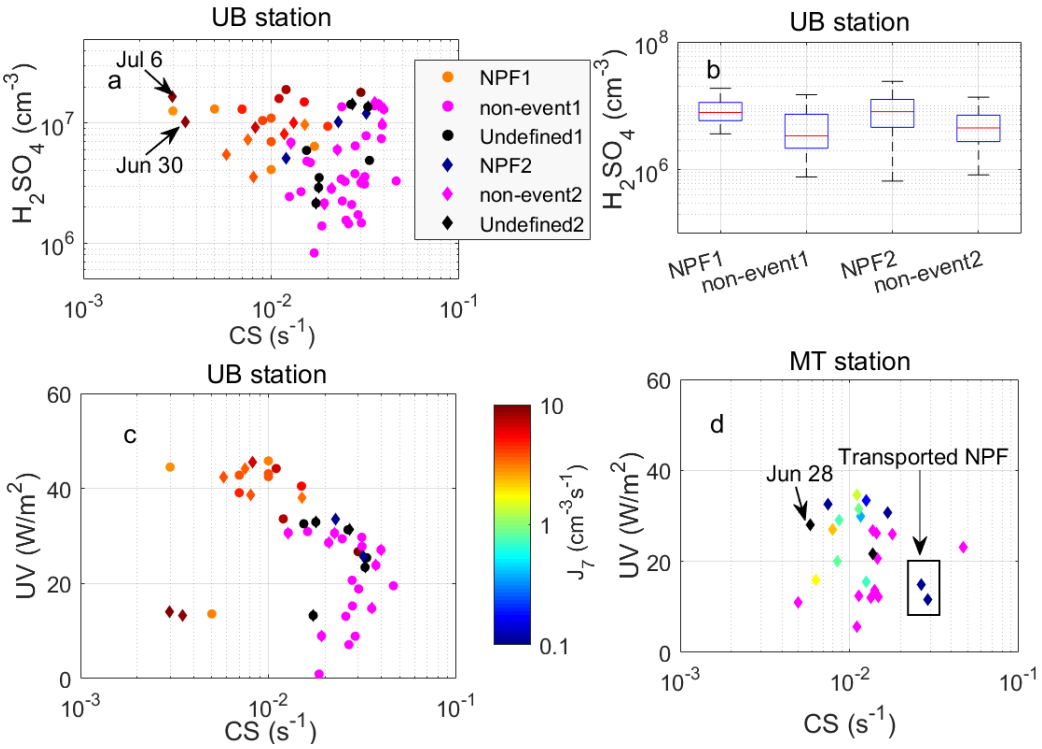

Figure R4-3: (a) Median condensation sinks (CS, s^{-1}) and H_2SO_4 concentration (cm^{-3}) and (b) median and percentiles of H_2SO_4 concentration observed at UB station during the first 2 hours of NPF events and 9:00-11:00 on non-event days, (c) solar radiation (UVA+UVB, W/m^2) during the first 2 hours of every NPF event and 9:00-11:00 on every non-event day at UB station. The 'NPF1' and 'non-event1' referred to NPF event and non-event days in summer 2018 and 2019 and the 'NPF2' and 'non-event2' referred to NPF event and non-event days during the observation from June 14 to July 14, 2019. (d) Median condensation sinks (CS, s^{-1}) and solar radiation (UVA+UVB, W/m^2) during the first 2 hours of every NPF event and 9:00-11:00 on every non-event day at MT station. Transported NPF event cases and one non-event day with air masses belonging to west group (Jun 28) were all pointed out in the figure. Color of data points on NPF event days means particle formation rate (J_7, $cm^{-3}s^{-1}$) when it can be calculated reliably. The time resolution of CS was 8 min at UB station and 4 min at MT station, respectively. The time resolution was 30 min for SA data at UB station and 1h for solar radiation data at both stations.

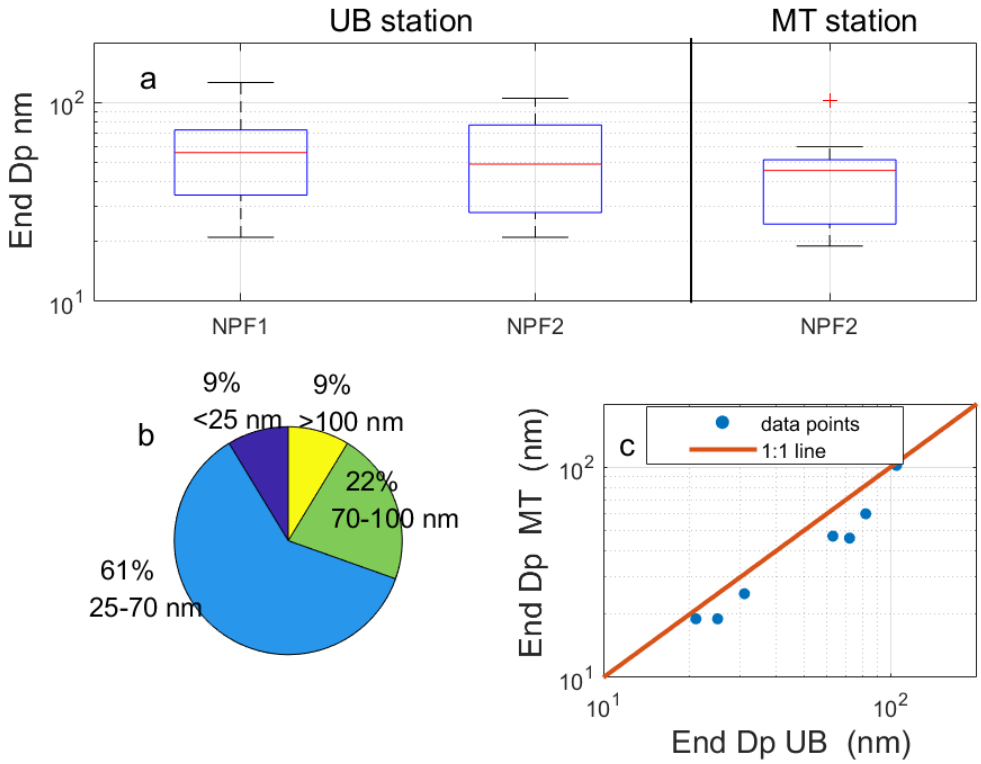

Figure R5-2: (a) Median and percentiles of end diameters (End Dp, nm) of NPF events measured at both sites. The red line represents the median of the data and the lower and upper edges of the box represent 25th and 75th percentiles of the data, respectively. The length of the whiskers represents 1.5× interquartile range which includes 99.3% of the data. The 'NPF1' and 'non-event1' referred to NPF event and non-event days in summer 2018 and 2019 and the 'NPF2' and 'non-event2' referred to NPF event and non-event days during the observation from June 14 to July 14, 2019. (b) Frequencies of end diameters in the size range of smaller than 25 nm, 25-70 nm, 70-100 nm and above 100 nm during our observation at UB station in summer 2018 and 2019. (c) Comparison between end diameters of common NPF events at both stations.

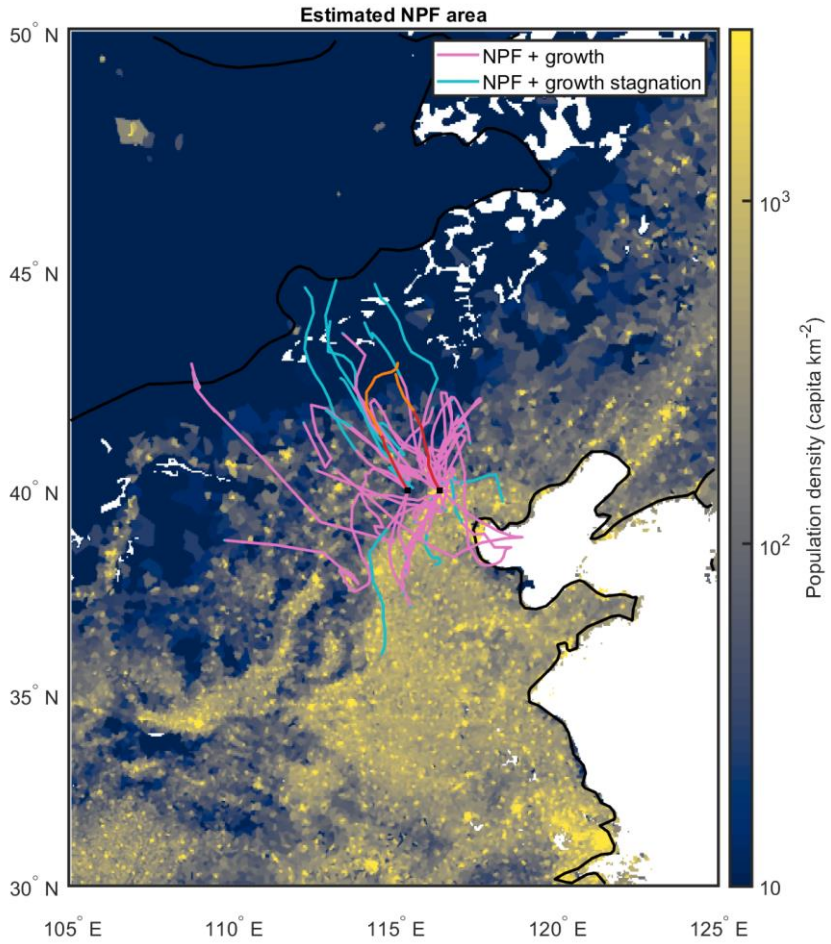

Figure R5-3: Spatial extent of the area where new particle formation events are estimated to have taken place based on air mass back trajectories and the observed NPF events at both sites. Each line represents a single NPF event and extends to the point beyond which continuation of the mode formed in an NPF event was no longer observed at the measurement site. In other words, if an air mass is located outside the area roughly outlined by the colored lines during the typical onset time of NPF and then transported to our measurement sites, NPF is unlikely to have occurred in said air mass. The lines change color from pink to light blue if the observed NPF event enters a stage of growth stagnation, which can indicate a less favorable environment for the formation and growth of new particles. The lines for the case study day of June 30, 2019 are marked with red and change color to orange if growth stagnation occurs. The lines are overlaid on top of a population density map (Gridded Population of the World; GPWv4.10; CC BY 4.0), which is used to illustrate the level of anthropogenic activities and emissions.

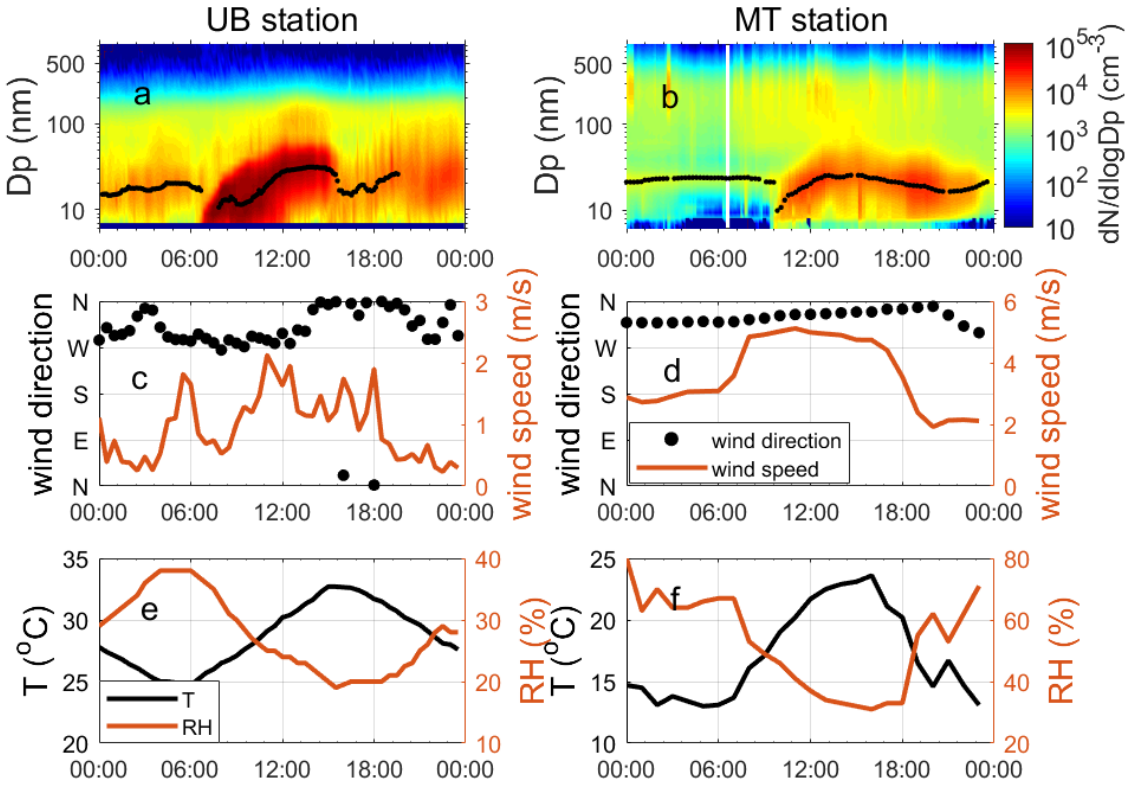

Figure R5-4: Time series of particle number size distribution and mode diameters (a, b), wind speed and direction (c, d), temperature and RH (e, f) measured at UB (left panel) and MT (right panel) on June 30, 2019.

References

Cai, R., Yang, D., Fu, Y., Wang, X., Li, X., Ma, Y., Hao, J., Zheng, J., and Jiang, J.: Aerosol surface area concentration: a governing factor in new particle formation in Beijing, Atmos Chem Phys, 17, 12327-12340, 10.5194/acp-17-12327-2017, 2017.

Deng, C., Cai, R., Yan, C., Zheng, J., and Jiang, J.: Formation and growth of sub-3 nm particles in megacities: impact of background aerosols, Faraday Discuss, 10.1039/d0fd00083c, 2020a.

Deng, C., Fu, Y., Dada, L., Yan, C., Cai, R., Yang, D., Zhou, Y., Yin, R., Lu, Y., Li, X., Qiao, X., Fan, X., Nie, W., Kontkanen, J., Kangasluoma, J., Chu, B., Ding, A., Kerminen, V. M., Paasonen, P., Worsnop, D. R., Bianchi, F., Liu, Y., Zheng, J., Wang, L., Kulmala, M., and Jiang, J.: Seasonal Characteristics of New Particle Formation and Growth in Urban Beijing, Environ Sci Technol, 54, 8547-8557, 10.1021/acs.est.0c00808, 2020b.

Hakala, S., Alghamdi, M. A., Paasonen, P., Vakkari, V., Khoder, M. I., Neitola, K., Dada, L., Abdelmaksoud, A. S., Al-Jeelani, H., Shabbaj, I. I., Almehmadi, F. M., Sundström, A.-M., Lihavainen, H., Kerminen, V.-M., Kontkanen, J., Kulmala, M., Hussein, T., and Hyvärinen, A.-P.: New particle formation, growth and apparent shrinkage at a rural background site in western Saudi Arabia, Atmos Chem Phys, 19, 19, https://doi.org/10.5194/acp-19-10537-2019, 2019.

Kangasluoma, J., Cai, R., Jiang, J., Deng, C., Stolzenburg, D., Ahonen, L. R., Chan, T., Fu, Y., Kim, C., Laurila, T. M., Zhou, Y., Dada, L., Sulo, J., Flagan, R. C., Kulmala, M., Petäjä, T., and Lehtipalo, K.: Overview of measurements and current instrumentation for 1–10 nm aerosol particle number size distributions, J Aerosol Sci, 148, 10.1016/j.jaerosci.2020.105584, 2020.

Kivekäs, N., Carpman, J., Roldin, P., Leppä, J., O'Connor, E., Kristensson, A., and Asmi, E.: Coupling an aerosol box model with one-dimensional flow: a tool for understanding observations of new particle formation events, Tellus B, 68, 29706, doi:10.3402/tellusb.v68.29706, 2016.

Kristensson, A., Johansson, M., Swietlicki, E., Kivekäs, N., Hussein, T., Nieminen, T., Kulmala, M., and Dal Maso, M.: NanoMap: geographical mapping of atmospheric new

particle formation through analysis of particle number size distribution data, Boreal Environ. Res., 19 (suppl. B), 329—342, 2014.

Kulmala, M., Kerminen, V. M., Petäjä, T., Ding, A. J., Wang, L.: Atmospheric gas-to-particle conversion: why NPF events are observed in megacities?, Faraday Discuss, 271-288, https://doi.org/10.1039/C6FD00257A, 2017.

Kulmala, M., Dada, L., Dällenbach, K., Yan, C., Stolzenburg, D., Kontkanen, J., Ezhova, E., Hakala, S., Tuovinen, S., Kokkonen, T., Kurppa, M., Cai, R., Zhou, Y., Yin, R., Baalbaki, R., Chan, T., Chu, B., Deng, C., Fu, Y., Ge, M., He, H., Heikkinen, L., Junninen, H., Nei, W., Rusanen, A., Vakkari, V., Wang, Y., Wang, L., yao, l., Zheng, J., Kujansuu, J., Kangasluoma, J., Petäjä, T., Paasonen, P., Järvi, L., Worsnop, D., Ding, A., Liu, Y., Jiang, J., Bianchi, F., Yang, G., Liu, Y., Lu, Y., and Kerminen, V.-M.: Is reducing new particle formation a plausible solution to mitigate particulate air pollution in Beijing and other Chinese megacities?, Faraday Discuss, 10.1039/d0fd00078g, 2021.

Liu, J. Q., Jiang, J. K., Zhang, Q., Deng, J. G., and Hao, J. M.: A spectrometer for measuring particle size distributions in the range of 3 nm to 10 mu m, Front Env Sci Eng, 10, 63-72, https://doi.org/10.1007/s11783-014-0754-x, 2016.

Lee, B. P., Li, Y. J., Flagan, R. C., Lo, C., and Chan, C. K.: Sizing characterization of the fast mobility particle sizer (FMPS) against SMPS and HR-ToF-AMS, Aerosol Sci. Technol., 47, 1030–1037, https://doi.org/10.1080/02786826.2013.810809, 2013.

Liu, J. Q., Jiang, J. K., Zhang, Q., Deng, J. G., and Hao, J. M.: A spectrometer for measuring particle size distributions in the range of 3 nm to 10 mu m, Front Env Sci Eng, 10, 63-72, https://doi.org/10.1007/s11783-014-0754-x, 2016.

Wang, Z. B., Hu, M., Sun, J. Y., Wu, Z. J., Yue, D. L., Shen, X. J., Zhang, Y. M., Pei, X. Y., Cheng, Y. F., and Wiedensohler, A.: Characteristics of regional new particle formation in urban and regional background environments in the North China Plain, Atmos Chem Phys, 13, 12495-12506, 10.5194/acp-13-12495-2013, 2013.

Ma, L., Zhu, Y., Zheng, M., Sun, Y., Huang, L., Liu, X., Gao, Y., Shen, Y., Gao, H., and Yao, X.: Investigating three patterns of new particles growing to the size of cloud condensation nuclei in Beijing's urban atmosphere, Atmos Chem Phys, 21, 183-200,

10.5194/acp-21-183-2021, 2021.

Man, H. Y., Zhu, Y. J., Ji, F., Yao, X. H., Lau, N. T., Li, Y. J., Lee, B. P., and Chan, C. K.: Comparison of Daytime and Nighttime New Particle Growth at the HKUST Supersite in Hong Kong, Environ Sci Technol, 49, 7170-7178, 2015.

Shen, X., Sun, J., Kivekäs, N., Kristensson, A., Zhang, X., Zhang, Y., Zhang, L., Fan, R., Qi, X., Ma, Q., and Zhou, H.: Spatial distribution and occurrence probability of regional new particle formation events in eastern China, Atmos Chem Phys, 18, 587-599, 10.5194/acp-18-587-2018, 2018.

Lampilahti, J., Manninen, H. E., Nieminen, T., Mirme, S., Ehn, M., Pullinen, I., Leino, K., Schobesberger, S., Kangasluoma, J., Kontkanen, J., Järvinen, E., Väänänen, R., Yli-Juuti, T., Krejci, R., Lehtipalo, K., Levula, J., Mirme, A., Decesari, S., Tillmann, R., Worsnop, D. R., Rohrer, F., Kiendler-Scharr, A., Petäjä, T., Kerminen, V.-M., Mentel, T. F., and Kulmala, M.: Zeppelin-led study on the onset of new particle formation in the planetary boundary layer, Atmospheric Chemistry and Physics Discussions, 10.5194/acp-2021-282, 2021.

Paasonen, P., Peltola, M., Kontkanen, J., Junninen, H., Kerminen, V.-M., and Kulmala, M.: Comprehensive analysis of particle growth rates from nucleation mode to cloud condensation nuclei in boreal forest, Atmos Chem Phys, 18, 12085-12103, 10.5194/acp-18-12085-2018, 2018.

Salma, I., Borsós, T., Weidinger, T., Aalto, P., Hussein, T., Dal Maso, M., and Kulmala, M.: Production, growth and properties of ultrafine atmospheric aerosol particles in an urban environment. Atmospheric Chemistry and Physics. 11. 10.5194/acp-11-1339-2011, 2011.

Zhang, J., Chen, Z., Lu, Y., Gui, H., Liu, J., Wang, J., Yu, T., and Cheng, Y.: Observations of New Particle Formation, Subsequent Growth and Shrinkage during Summertime in Beijing, Aerosol Air Qual Res, 16, 1591-1602, 10.4209/aaqr.2015.07.0480, 2016.